ISSN 0018-1439, High Energy Chemistry, 2016, Vol. 50, No. 2, pp. 144–149. © Pleiades Publishing, Ltd., 2016.
Original Russian Text © A.V. Tatarinov, Yu.A. Lebedev, I.L. Epstein, 2016, published in Khimiya Vysokikh Energii, 2016, Vol. 50, No. 2, pp. 149–154.

PLASMA CHEMISTRY

Simulation of Microwave-Induced Formation of Gas Bubbles in Liquid *n*-Heptane

A. V. Tatarinov[a], Yu. A. Lebedev[a], and I. L. Epstein[a, b]

[a] *Topchiev Institute of Petrochemical Synthesis, Russian Academy of Sciences, Leninskii pr. 29, Moscow, 119991 Russia*
e-mail: lebedev@ips.ac.ru

[b] *Moscow Institute of Physics and Technology (State University), Institutskii per. 9, Dolgoprudnyi, Moscow oblast, 141700 Russia*

Received April 27, 2015; in final form, July 28, 2015

Abstract—A model has been built and the formation of gas bubbles by exciting an atmospheric-pressure microwave discharge in liquid *n*-heptane has been numerically simulated in the approximation of axial symmetry. The model is based on the simultaneous solution of Maxwell's equations, Navier–Stokes equations, the heat conduction equation, a balance equation for the electron number density (using the ambipolar diffusion approximation), Boltzmann's equation for free plasma electrons, and the overall equation for the thermal degradation of *n*-heptane. The two-phase medium has been described using the phase field method. The calculation has made it possible to describe both the dynamics of the formation of gas bubbles in the liquid and the thermal processes in the system. The calculated gas temperature in the gas bubble with the plasma is in agreement with the measurement results.

Keywords: microwave discharge, *n*-heptane, mathematical modeling, two-phase fluid
DOI: 10.1134/S0018143916020077

n the last decade, studies on microwave (MW) discharge in gas bubbles in liquids including liquid hydrocarbons, such as *n*-dodecane [1–4]; benzene [2]; cooking oil, machine oil, and waste oils [2]; silicone oil [3]; methylene blue-containing water [5, 6]; an aqueous trichloroethylene solution [6]; and *n*-heptane [7, 8], have been reported. Pioneering works on the simulation of such discharges [7] and their spectral diagnostics [9, 10] have also been published. The reason for interest in this type of discharge is believed to be the possibility of producing hydrogen, coatings, nanoparticles, and nanotubes. Since plasma occurs inside the liquid, physicochemical processes due to the action of active plasma species and plasma radiation are highly effective. Accordingly, the product formation rates are also high. However, there is a lack of real data to determine the prospects of using MW discharge. In all of the studies cited above, microwave discharges excited with various types of antenna were used to generate plasma. Gas bubbles are produced by either evaporating the liquid, or bubbling a gas (argon), or ultrasonic cavitation. Summarizing the results, one can say that the discharge system is essentially nonequilibrium and holds promise as an effective means of running plasma-chemical reactions. However, the relevant data are scanty and no systematic studies have been carried out yet.

The experimental setup used in this study is detailed in [7, 8, 10]. It consisted of a metal chamber to which microwave power was supplied from a magnetron (2.45 GHz, 500 W) with the use of a rectangular waveguide. The chamber was placed in a heat-resistant glass cup with a quarter-wave MW antenna mounted on a metal base. Saturated C_7–C_{16} hydrocarbons were poured into the cup (of about 50 mL in volume) to completely cover the antenna. When microwave power was applied, the hydrocarbon evaporated in the area of maximum MW field strength at the end of the antenna and microwave discharge was initiated in the gas bubble produced. Emission spectra in the wavelength range of 200 to 800 nm were investigated. They appeared to be similar for all of the hydrocarbons. The spectra consisted of a broad continuum with superimposed Swan bands of the C_2 molecule. The rotational (gas) temperature determined by processing the spectra was 1600 ± 200 K.

This work is in continuation of the research in this field at the Topchiev Institute of Petrochemical Synthesis [7, 8, 10] and deals with the first step of simulation of this type of discharge concerning the description of the formation of vapor bubbles in *n*-heptane and microwave plasma generation at atmospheric external pressure. The main purpose of the study was to describe the thermal processes occurring in *n*-heptane.

MATHEMATICAL MODEL

We solve a two-dimensional axisymmetric problem with a cylindrical working chamber, in which a cylindrical cup with quartz walls is placed. The cup contains liquid *n*-heptane. The energy from the microwave source is fed from the bottom through a coaxial cable. The calculation assumes that the cup walls are infinitely thin and coincide with the metal walls of the working chamber, except for microwave-transparent area AB (Fig. 1). In addition, there is a small cylindrical cavity on the bottom of the "cup." Initially, the lower part of the cavity is filled with superheated vapor. This part is responsible for the nucleation of the superheated vapor bubble involved in the further boiling process. An *n*-heptane gas plasma appears in the bubble, leading to local heating and growth of the bubble. The position of the interface between the liquid and gas phases changes with time.

The process of bubble formation and boiling was analyzed using the phase-field method [11, 12]. The method is a variant of the single-fluid approach to the modeling of two-phase flow, in which both phases are described by Navier–Stokes equations and the boundary between the two media is assumed to have a finite thickness and be characterized by fast, but smooth change in density, velocity, and other physical parameters. For transition between the phases, a dimensionless phase indicator function φ ($-1 \le \varphi \le 1$, $\varphi = -1$ for the vapor phase, $\varphi = 1$ for the liquid phase) determined from the Cahn–Hilliard equation is introduced. The total free energy of the system is determined from the Ginzburg–Landau relation.

The calculations used a two-dimensional axisymmetric model that included a system of Navier–Stokes equations for two-phase subsonic flow of incompressible fluid and compressible gas, heat conduction equation, Maxwell's equation for the microwave field, and the balance equation for electron number density.

Maxwell's Equations

In the case of a stationary structure of transverse magnetic (TM) waves, Maxwell's equations are reduced to the solution of a single complex equation for the magnetic component of the wave:

$$\nabla \times ((\varepsilon_r - j\sigma/\omega\varepsilon_0)^{-1}\nabla \times \mathbf{H}_\varphi) - \mu_r k_0^0 \mathbf{H}_\varphi = 0. \quad (1)$$

Here, $\varepsilon_r = 1 - n_e/n_c$ is the relative permittivity of plasma; σ is the electrical conductivity of the plasma: $\sigma = f_{\text{col}}\varepsilon_0 n_e/n_c$, f_{col} is the frequency of collisions of electrons with neutrals, ε_0 is the permittivity of vacuum; n_c is the normalizing number density of electrons, $n_c \approx 3 \times 10^{15}$ cm^{-3} for the given microwave frequency of $f =$ 2.45 GHz; and $k_0 = 2\pi f/c$ is the wave vector. Relative magnetic conductivity μ_r of the medium is unity.

Fig. 1. Calculation domain and distribution of *n*-heptane liquid and vapor phases at the initial point of time. T-shaped segment A–B is permeable to microwaves and impermeable to *n*-heptane.

Navier-Stokes Equations

$$\rho\frac{\partial u}{\partial t} + \rho(\mathbf{u}\cdot\nabla)\mathbf{u} = \nabla[-p\mathbf{I} + \eta(\nabla\mathbf{u} + (\nabla\mathbf{u})^T)] + \rho\mathbf{g} + G\nabla\varphi, \quad (2)$$

$$\nabla \cdot \mathrm{u} = \dot{m}\delta\left(\frac{1}{\rho_V} - \frac{1}{\rho_L}\right). \quad (3)$$

Here, G is the chemical potential, η is the dynamic viscosity; p is the pressure; ρ is the density; L denotes the liquid phase, v refers to vapor; $\dot{m}$. is the liquid evaporation rate; δ is the curvature of the interface between the two phases, $\delta = 6V_{jL}V_{fV}\frac{|\nabla\varphi|}{2}$, V_{fv} V_{fL} are the volume fractions of the vapor and liquid, respectively. The density of the medium is determined as $\rho = V_{fL}\rho_L + V_{fv}\rho_V$, where ρ_L and ρ_V are the densities of the liquid and vapor, respectively. The vapor density is determined from the equation of state of ideal gas.

Along with the pressure, viscosity, and buoyancy forces, the surface tension written as spatial source $G\nabla\varphi$ is taken into account:

$$G = \frac{\lambda}{\varepsilon^2}(-\nabla\varepsilon^2\nabla\varphi + (\varphi^2 - 1)\varphi). \quad (4)$$

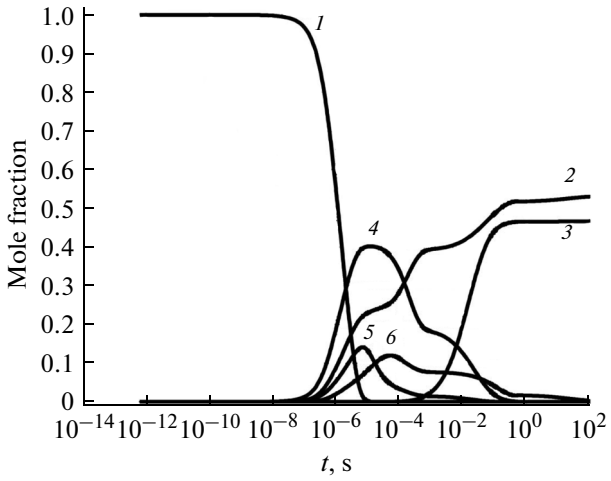

Fig. 2. Mole fractions of the main products of *n*-heptane pyrolysis at $T = 1500$ K as a function of time: (*1*) C_7H_{16}, (*2*) H_2, (*3*) C, (*4*) C_2H_4, (*5*) C_3H_6, and (*6*) CH_4. Calculation.

Here, λ is the energy density of mixing of the media and ε is the characteristic size of the capillary that determines the interface thickness scale. The two latter parameters are related to surface tension σ_s by $\sigma_s = (2\sqrt{2}/3)\lambda/\varepsilon$.

The value of $\dot{m}$. is found from the heat flux at the interface

$$\dot{m} = -\left(\frac{M_w}{\Delta H_{vl}}\right)\mathbf{n}\cdot k_V \nabla T_V. \quad (5)$$

where M_w is the molecular weight of vapor, ΔH_{vl} is the enthalpy of vaporization, k is the thermal conductivity coefficient, and n is the unit vector normal to the interface.

Cahn–Hilliard Equation for φ

$$\frac{\partial \varphi}{\partial t} + \mathbf{u}\cdot\nabla\varphi - \dot{m}\delta\left(\frac{V_{fL}}{\rho_L} + \frac{V_{fV}}{\rho_V}\right) = \nabla\cdot\frac{\gamma\lambda}{\varepsilon^2}\nabla\psi. \quad (6)$$

Here, ψ is an auxiliary variable, $\psi = -\nabla\varepsilon^2\nabla\varphi + (\varphi^2 - 1)\varphi$, γ is the mobility, which determines the time scale of Cahn–Hilliard diffusion.

Heat Equation

$$\rho c_p\frac{\partial T}{\partial t} + \rho c_p(\mathbf{u}\cdot\nabla)T + \nabla\cdot(-k\nabla T) = Q_s + Q_{chem} - \frac{\dot{m}}{M_w}\delta\Delta H_{Vl}. \quad (7)$$

The terms in the right-hand side of Eq. (7) take account of gas heating by a microwave field, the heat of chemical reactions, and the temperature change due to evaporation of the liquid. Here, c_p and k are the heat capacity and thermal conductivity of the mixture, respectively, determined with allowance for the volume fraction of each phase:

$$c_p = V_{fL}c_{pL} + V_{fV}c_{pV},$$
$$k = V_{fL}k_L + V_{fV}k_V,$$

Q_s is the heat source associated with microwave power consumed for heating the plasma: $Q_s = \alpha\sigma\left|E_m^2\right|$, α is the proportion of microwave energy converted into heat. In calculations, the value of α was varied from 0.1 to 1.0. Q_{chem} is the heat of reaction of the thermal degradation of *n*-heptane.

To determine Q_{chem}, the kinetics of the pyrolysis of *n*-heptane at different gas temperatures was preliminarily calculated. The reaction scheme given in [13] was used. It includes 47 components and 374 reactions. Figure 2 presents the results of calculation for a temperature of 1500 K. The main components of *n*-heptane degradation at different times are shown. In the first step of the calculation, the formation of the solid phase was not taken into account. The two-dimensional model included only the initial stage of heptane degradation accompanied by a sharp drop in temperature, which in turn could lead to a change in the pattern of flow through the change in density. Meant by the initial stage is the period of time during which the concentration of *n*-heptane drops by more than three orders of magnitude. The *n*-heptane degradation process is initiated by monomolecular C–C bond dissociation into two alkyl radicals and, to a lesser extent, C–H bond breaking to form the hydrogen atom and various alkyl radicals. The degradation involves *n*-heptane reactions with radical species (H atom and CH_3 and C_2H_5 alkyl radicals). The C_7H_{15} radicals thus formed generally decompose into an olefin (ethylene) molecule and an alkyl radical with a smaller number of carbon atoms. The analysis showed that the principal process occurring at all the temperatures examined is the interaction of the H atom with *n*-heptane. Since the concentration of H atoms depends on many other processes and varies with time, it appears impossible to directly simulate in terms of the spatial model the rate *n*-heptane pyrolysis involving the H atom. Therefore, we used a simplified approach. Figure 3a shows the time dependence that we have calculated for *n*-heptane concentrations at different temperatures; this relation made it possible to roughly estimate the characteristic time of *n*-heptane degradation, τ_x, depending on the gas temperature (Fig. 3b). The *n*-heptane degradation rate was written as $r_h = [C_7H_{16}]/\tau_x$. In order to calculate the heat of the overall reaction of *n*-heptane degradation, it is necessary to know its products. Based on our kinetic calculations, we assumed that the products are CH_4, C_2H_4, C_3H_6, and H_2. The overall reaction for the formation for these products can be written as:

$$3C_7H_{16} \rightarrow CH_4 + 7C_2H_4 + 2H_2 + 2C_3H_6. \quad (8)$$

The energy decrease in Eq. (7) is determined by the heat of reaction (8) of the thermal degradation of *n*-heptane: $Q_{chem} = -H_h r_h$, where H_h and r_h are respectively the enthalpy and the rate of the *n*-heptane degradation reaction.

Balance Equation for Electron Number Density

$$\frac{\partial n_e}{\partial t} + \nabla \cdot (-D_{am}\nabla h_e + n_e \mathbf{u}) = k_i\left(\frac{E}{N}\right)[C_7H_{16}]n_e - k_{rec}n_e^2. \quad (9)$$

Here, D_{am} is the ambipolar diffusion coefficient, $D_{am} \approx \mu_i\varepsilon_x$ [14]; k_i and k_{rec} are the rate coefficients of ionization of *n*-heptane and bulk recombination of the *n*-heptane principal ion, respectively; μ_i is the mobility of the principal ion; and ε_x is its characteristic energy.

To determine the ionization rate coefficient, the electron energy distribution function (EEDF) was calculated. The Boltzmann equation for the stationary, isotropic part of EEDF written in the binomial approximation of distribution expansion in spherical harmonics was used. Unfortunately, the self-consistent set of *n*-heptane cross sections required for calculating the EEDF is unknown. In such cases, the kinetics of electrons in heavy hydrocarbons is described using a known set of cross sections for a lighter hydrocarbon [15]. Thus, according to published data [16], the cross sections of vibrational and electronic excitation of saturated C_3–C_7 hydrocarbons are close. Therefore, in a first approximation, we used the set of cross sections for propane [17]. To calculate the ionization constants for *n*-heptane, the total ionization cross section measured in [18] was used. Vacher et al. [18] also measured partial ionization cross sections of *n*-heptane. It was shown that the most abundant ion near the ionization threshold (~10 eV) is the molecular ion $C_7H_{16}^+$, and that above 16 eV is the $C_3H_7^+$ ion. The analysis based on the EEDF calculated in the present study shows that $C_7H_{16}^+$, can be regarded as the principal ion accurate to within ~20% in the *E/N* range relevant to this work (<400 Td). The mobility of this ion was calculated using the following approximate expression for the ion mobility in the parent gas [19]:

$$\mu = \frac{0.341e}{N\sigma_{res}(2.13v_T)\sqrt{MT}},$$

where *e* is the electron charge, *M* is the mass of the ion, *N* is the number of neutrals, $(2.13v_T)$ is an independent variable indicating the velocity at which the cross section is to be taken, and $v_T = \sqrt{2T/M}$ is the thermal velocity of the ion. Cross section σ_{res} of resonant charge exchange was evaluated using the relation $\sigma_{res} = \frac{\pi}{2}\frac{\hbar^2}{2Ml}\ln^2\left(\frac{100}{v}\sqrt{\frac{2I}{M}}\right)$ [14] where v is the velocity of the ion, I is the ionization potential, and $\hbar$ is Planck's constant. For the electron–ion recombination rate constant, the expression $k_{rec} = 3.5 \times 10^{-8}/T_e^{0.68}$ [cm^3/s] [20] was used, where T_e is the electron temperature in eV.

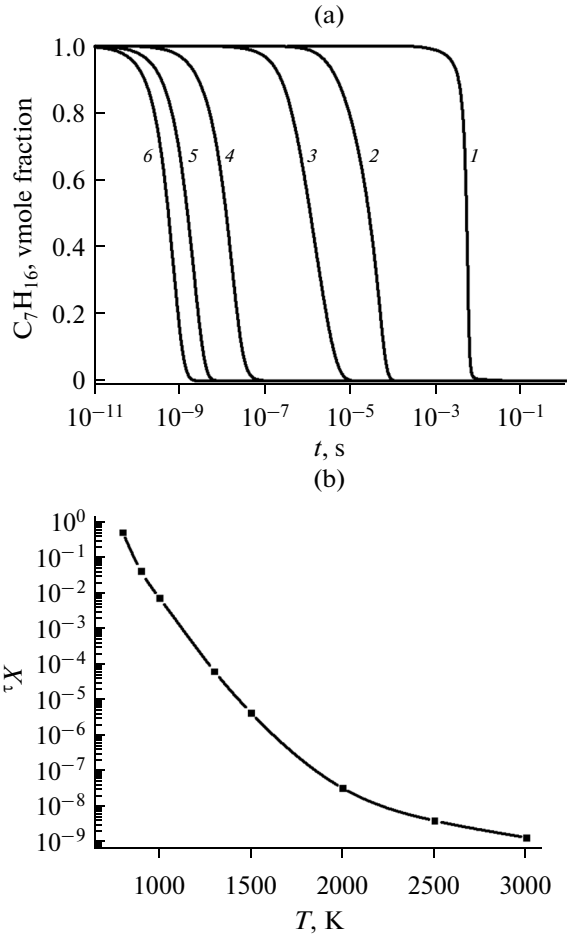

Fig. 3. (a) Calculated time dependence of the *n*-heptane concentration during pyrolysis for various gas temperatures (*T*): (*1*) 1000, (*2*) 1300, (*3*) 1500, (*4*) 2000, (*5*) 2500, and (*6*) 3000 K. (b) Temperature dependence of the characteristic time of the overall *n*-heptane degradation reaction. Calculation.

The simulation was performed by the finite element method using the program Comsol 3.5a [21]. The computations were made with a 12-core Xeon processor having a frequency of 2.3 GHz and 32 GB of RAM.

RESULTS

The calculation makes it possible to trace the evolution of the boiling process. At the initial time, a small

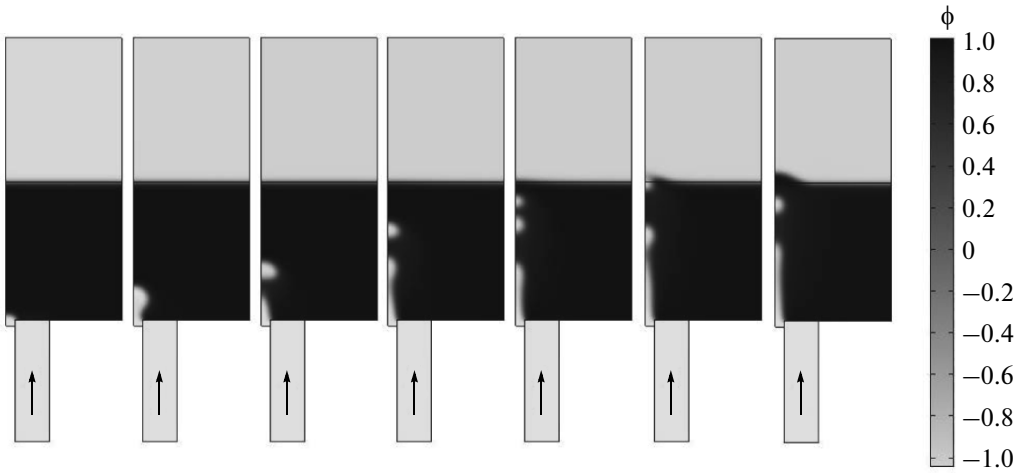

Fig. 4. Phase diagrams at different times of (left to right) 0.004, 0.035, 0.07, 0.105, 0.14, 0.175, and 0.2 s and an incident power of 500 W; $\varphi = -1$ (vapor), $\varphi = 1$ (liquid).

bubble of superheated gas inside the cavity is defined. The scenario of the further process strongly depends on an incident microwave powerP_0. There can be modes when the bubble disappears, expands and remains in place, or converts into a column of superheated vapor.

In the intermediate power range, the mode of the periodic formation of bubbles and their subsequent rising to surface is possible. Figure 4 shows a flow pattern at different points of time for this case. Note that the calculations made it possible to determine the characteristic times of the formation of the bubble ($\sim 10^{-3}$ s), its separation ($\sim 10^{-2}$ s), and subsequent floating up ($\sim 10^{-1}$ s). The diameter of the resulting bubbles is comparable with the cavity diameter. In the given case, it is several millimeters. The bubble floating-up speed is about one meter per second. The velocity of the liquid during stirring is much lower, being about a centimeter per second. The plasma operates only inside the cavity, in the vicinity of the central electrode. The plasma in bubble is extinguished when the bubble detaches from the electrode. The disappearance of the plasma is due to the fact that the microwave field concentrates near the face end of the central electrode and very sharply falls outside it (Fig. 5). At a power of 500 W, the MW field strength at the end of the electrode can be as high as ~10.000 V/cm. Our three-dimensional calculation of the microwave field for the working chamber described in [10] gave values of the same order of magnitude. Since the plasma parameters depend on the MW field strength, there are grounds to consider that the results obtained in this study are comparable with those reported in [10]. The gas temperature in the vicinity of the central conductor of the coaxial line, which is determined by the absorption of microwave energy in the plasma and endothermicity of the *n*-heptane decomposition reaction, is ~1100–1600 K. This value is consistent with the gas temperature found experimentally [10]. Note that varying the proportion of microwave energy consumed for heating the gas (α) from 0.1 to 1.0 leads to a change in the gas temperature by no more than 300 K. The maximum number density of electrons is approximately 10^{14} cm^{-3}. Figure 5 shows the axial profiles of the gas-phase proportion, the gas temperature, and the magnitude of the MW field at the bubble detachment time. It can be seen that during its rising to the surface, the bubble quickly cools by virtue of evaporation of the boiling liquid into the bubble and its temperature becomes approximately equal to the boiling point. The axial profile of the microwave field confirms our previous conclusions about the dramatic drop in the MW field outside the cavity. The presence of a small peak of MW field near the top of the bubble seems to be due to the jump in dielectric permittivity at the interface between the liquid and gas phases.

CONCLUSIONS

Pioneering results in the simulation of microwave discharge in liquid *n*-heptane have been presented. On their basis, it has become possible to study the thermal processes in the system leading to the formation of gas bubbles by excitation of the discharge and to determine the characteristic time and dynamics of the evaporation process. It is planned to extend the kinetic scheme of the processes in plasma for taking detailed account of not only the thermal and electron impact-induced processes, but also the formation of the solid phase.

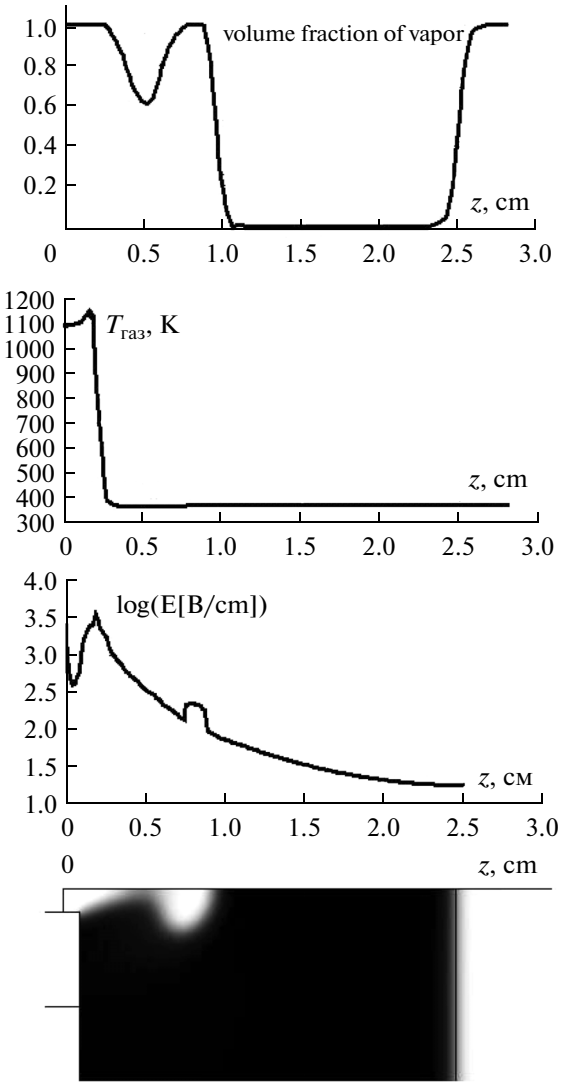

Fig. 5. Panels from left to right: axial profiles ($r = 0$) of the volume fraction of the gas phase, the gas temperature, and the microwave field strength at a time of $t = 0.055$ s and an incident power of 500 W. Right panel: phase diagram of *n*-heptane corresponding to this point in time.

ACKNOWLEDGMENTS

The work was supported by the Russian Ministry of Education and Science, project no. RFMEF157514X0060.

REFERENCES

1. Nomura, S. and Toyota, H., *Appl. Phys. Lett.*, 2003, vol. 83, p. 4503.
2. Nomura, S., Toyota, H., Tawara, M., Yamashita, H., and Matsumoto, K., *Appl. Phys. Lett.*, 2006, vol. 88, p. 231502.
3. Nomura, S., Toyota, H., Mukasa, S., Yamashita, H., Maehara, T., and Kuramoto, M., *Appl. Phys. Lett.*, 2006, vol. 88, p. 211503.
4. Nomura, S., Toyota, H., Mukasa, S., Yamashita, H., Maehara, T., and Kawashima, A., *J. Appl. Phys.*, 2009, vol. 106, p. 073306.
5. Ishijima, T., Sugiura, H., Satio, R., Toyada, H., and Sugai, H., *Plasma Sources Sci. Technol.,* 2010, vol. 19, p. 015010.
6. Ishijima, T., Hotta, H., and Sugai, H., *Appl. Phys. Lett.,* 2007, vol. 91, p. 121501.
7. Buravtsev, N.N., Konstantinov, V.S., Lebedev, Yu.A., and Mavlyudov, T.B., *Microwave Discharges: Fundamentals and Applications (Proceedings of VII International Workshop, September10–14, 2012, Zvenigorod, Russia)*, Lebedev, Yu.A., Ed., Moscow: YanusK, 2012, p. 167.
8. Lebedev, Yu.A, Konstantinov, V.S., Yablokov, M.Yu., Shchegolikhin, A.N., and Surin, N.M., *High Energy Chem.*, 2014, vol. 48, p. 385.
9. Camerotto, E., De Schepper, R., and Nikiforov, A.Y., *J. Phys. D: Appl. Phys.*, 2012, vol. 45, p. 435201.
10. Lebedev, Yu.A., Epstein, I.L., Shakhatov, V.A., Yusupova, E.V., and Konstantinov, V.S., *High Temp.*, 2014, vol. 52, p. 319.
11. Sun, Y. and Beckermann, C., *Physica D (Amsterdam),* 2004, vol. 198, p. 281.
12. Jamet, D., http://pmc.polytechnique.fr/mp/GDR/docu/Jamet.pdf
13. Curran, H.J., Gaffuri, P., Pitz, W.J., and Westbrook, C.K., *Combust. Flame*, 1998, vol. 114, p. 149.
14. Raizer, Yu.P., *Fizika gazovogo razryada* (Gas Discharge Physics), Moscow: Nauka, 1987.
15. Kosarev, I.N., Aleksandrov, N.L., Kindysheva, S.V., Starikovskaia, S.M., and Starikovskii, A.Yu., *Combust. Flame*, 2009, vol. 156, p. 221.
16. Slovetskii, D.I., *Khim. Plazmy*, 1981, issue 8, p. 189.
17. *Morgan Database*, www.lxcat.net
18. Vacher, J.R., Jorand, F., Blin-Simiand, N., and Pasquiers, S., *Int. J. Mass Spectrom.*, 2010, vol. 295, p. 78.
19. McDaniel, E. and Mason, E., *The Mobility and Diffusion of Ions in Gases*, New York: Wiley, 1973.
20. *Entsiklopediya nizkotemperaturnoi plazmy* (Encyclopedia of Low-Temperature Plasma) Fortov, V.E, Ed., Moscow: Nauka, 2000, vol. 1, sect. II.4.5.
21. *COMSOL 3.5a*, http://www.comsol.com

Translated by S. Zatonsky

SPELL: 1. Насыщенный пар